International Journal of Applied Pharmaceutics

ISSN- 0975-7058 Vol 16, Issue 6, 2024

Original Article

IMPACT OF LIGAND CONJUGATION OF PHYSICOCHEMICAL ATTRIBUTES OF POLYMERIC NANOPARTICLES OF ATYPICAL ANTIPSYCHOTIC DRUG FOR NOSE-TO-BRAIN DELIVERY

TEJA KUMAR PONDURI[1*], CHAKRAVARTHI GUNTUPALLI[1], BALAMURUGAN JEGANATHAN[2], NARENDER MALOTHU[1]

[1]KL College of Pharmacy, Koneru Lakshmaiah Education Foundation, Vaddeswaram, Andhra Pradesh, India. [2]Formulation Development, Zhejiang Heze Pharmaceutical Technology Co., Ltd., 101, No. 1 Street, Qiantang New District, Hangzhou, Zhejiang. PR China
*Corresponding author: Teja Kumar Ponduri; *Email: tejpharmandhra@gmail.com

Received: 30 Apr 2024, Revised and Accepted: 28 Sep 2024

ABSTRACT

Objective: To formulate and characterize the ligand-conjugated chitosan nanoparticles of Ziprasidone Hydrochloride (ZH) and compare with its plain chitosan nanoparticles.

Methods: Transferrin (Tf) conjugated Chitosan Nanoparticles (CH-NP) containing ZH were prepared by ionotropic gelation method by using modified chitosan and Tf. Physicochemical attributes of nanoparticles which can potentially impact the nose-to-brain delivery were evaluated.

Results: The Tf-CH-NP has demonstrated 207.1 nm mean particle size, 87.6% entrapment efficiency with a release of 89.34% at 24 h and has shown about 2.22 times more release than drug suspension and about 4.5% more than plain CH-NP. The similar trend was observed in Ex vivo nasal permeation study. Its acceptability was shown in histomorphology study, where a minimal inflammation seen, that might be due to the pH of the formulation. There is deeper penetration with Tf-CH-NP, which is more promising for penetration into brain.

Conclusion: The formulated Tf-CH-NP has a greater potential due to ligand conjugation to reach the brain and, facilitate targeted delivery and enables better treatment of schizophrenia at minimal doses.

Keywords: Ziprasidone, Ligand conjugated nanoparticles, Transferrin, Chitosan, Click reaction, Nose to cerebrum

DOI: https://dx.doi.org/10.22159/ijap.2024v16i6.52003 Journal homepage: https://innovareacademics.in/journals/index.php/ijap

INTRODUCTION

Schizophrenia is a Central Nervous System (CNS) related health condition affecting less than1% of global population but it caused the loss of 28.5 years of life impacting the behaviour, feelings and thinking of people [1]. During the treatment of schizophrenia by using Antipsychotics, patients are experiencing extrapyramidal side effects, weight gain and metabolic syndrome, which is varying with the specific medication [2]. The "Intranasal administration" of drugs when formulated as nanosized particles holds promise for higher efficiency in reaching cerebral tissues and also provide benefits of protecting the drugs from degradation [3–6].

"Ziprasidone Hydrochloride" (ZH), an atypical antipsychotic drug and dopamine D2 antagonist, indicated for the treatment of schizophrenia [2, 4, 7]. It has poor bioavailability (60%), which is limited by its solubility and higher first-pass metabolism. Consistent efforts were made to improve the solubility and bioavailability by formulating as novel drug delivery systems [4, 6, 8–12].

The nanoparticle formulation of Ziprasidone using Chitosan crosslinked with sodium tripolyphosphate and by ionic gelation method has shown potential of improved bioavailability. In the present study, a brain-targeting ligand was crosslinked to the chitosan nanoparticles and its characteristics were evaluated and compared with nanoparticles to evaluate the impact of ligand conjugation on nose to brain drug delivery. "Transferrin" (Tf) has been investigated as a targeting ligand using "Strain-Promoted Azide-Alkyne Cycloaddition" (SPAAC) reaction with the aim of potentially applying them to improve quality of life of schizophrenic patients [13–15].

MATERIALS AND METHODS

Materials

Ziprasidone Hydrochloride is gift sample from Wuxi DEC pharma, Wuxi, China. Fluorescein azide was from Hangzhou MolCore BioPharmatech Co., Ltd., Zhejiang, China. Remaining all materials are from Sangon Biotech (Shanghai) Co., Ltd., Shanghai, China. The Wuxi DEC laboratory supplied the analytical grade solvents and chemicals utilized in the experiments.

Methods

To synthesize conjugated chitosan nano sized particles, it is necessary to modify the chitosan by introducing azide groups, resulting in azido-chitosan. Additionally, the transferrin molecule needs to undergo modification by incorporating an alkyne group [13–17].

Modification of chitosan (Azidation)

Chitosan underwent modification using the process published by *Gabold et al.* with minor adjustments [13–17]. By dissolving 5-azidopentanoic acid (0.78 g), a colorless to yellow liquid, and chitosan (1.0 g) in 50 ml of 2-Morpholino Ethane Sulfonic Acid Buffer (MES buffer), a mixture was prepared. The prepared mixture was stirred at ambient room temperature for a duration of 6 h. To remove any traces of oxygen, the solution was subjected to nitrogen sparging for 45 min. Within a span of half an hour, 3.14 g of EDAP Carbodiimide (EDC) and 5.66 g of N-Hydroxysuccinimide (NHS) were added to the flask and stirred for 16 h to allow the reaction to take place. The polymer solution was then subjected to dialysis using a standard grade RC membrane (8 KD, flat width 40 mm, volume 5.1 ml/cm) and distilled water for one week in ice batch at 2-8 °C to eliminate impurities. Finally, the obtained solution was lyophilized to get dried form of azide functionalized Chitosan (0.97 g) as a slightly yellow powder, with a yield of 54.7% w/w.

Modification of transferrin (Alkynation)

Transferrin underwent alkylation following the process published by *Gabold et al.* with minor adjustments [13–15]. In a test tube, 60 mg of Human holo-Transferrin, which was produced in rice, was dissolved in 1.8 ml of phosphate buffer at pH 8.0. In another test tube, 3.28 mg of "DBCO-NHS ester" "(Dibenzyl Cyclooctyne-N-Hydroxy Succinimide-Ester)" dissolved in 0.2 ml of Dimethyl sulfoxide was then added to the Transferrin solution and stirred all night at 400rpmin ice bath at 2-8 °C. The resulting conjugate was

purified through "pre-packed PD-10 desalting column" filled with "Sephadex G-25 resin" and subsequently lyophilized. As a final product, 52.3 mg of alkyne-functionalized Transferrin was obtained, yielding 82.5% (w/w), and appeared as a pale red powder.

Preparation of nano sized particles

Nano-sized particles were prepared following the process published by *Gabold et al.* with minor adjustments [13, 18]. In the synthesis of surface-modified CH nano-sized particles, previously prepared azide-modified chitosan and regular chitosan were combined in equal parts to achieve 2.5 mg/ml in 5.0 pH Acetate buffer. The chitosan mixture underwent filtration using a 0.45-µm Cellulose nitrate Ester filter. Alkyne functionalized Tf solutions of 1 mg/ml to 5 mg/ml were prepared with highly purified water. 1 mg/ml of ZH solution prepared with Glacial acetic acid was then added to the chitosan mixture. 2 mg/ml of Penta sodium tripolyphosphate solution prepared with highly purified water and added to chitosan mixture. After the incorporation of the crosslinking agent and drug substance into the chitosan solution, the mixture was stirred for a duration of 60 min at 14000 rpm prior to the introduction of 1 ml of alkyne-modified Tf at the corresponding concentration. The resulting dispersion was sonicated for 8 min. The nano sized particles were then subjected to centrifugation for a duration of 60 min at a speed of 10,000 rpm on a glycerol bed measuring 20µl*, following which the supernatant was carefully poured off.

***In vitro* characterization of nano-sized particles**

Hydrodynamic diameter, zeta potential and PDI

The hydrodynamic diameter and Polydispersity Index (PDI) were measured using dynamic light scattering, and laser doppler anemometry was employed to analyse the zeta potential. A disposable micro-cuvette (Malvern Instruments, Malvern, UK) was filled with 100 µl** of Nano-Sized Particles (NPs) suspended in ultra-purified water. Further, using a Zetasizer Nano ZS (Malvern Instruments) at a 173° backscatter angle three times for each sample to measure the size and PDI. Data analysis was conducted using the Zetasizer software, with a viscosity of 0.88 mPass and a refractive index of 1.33 set appropriately. The NPs were then diluted with 900 µl of 10 mmol sodium chloride, and 700 µl of the NP suspension was put into a capillary that had been folded [19].

Surface morphology by transmission electron microscopy (TEM)

"The Transmission Electron Microscopy" (TEM) technique was employed to conduct a surface morphological examination of blank NPs, Tf-CH-NPs, and CH-NPs of ZH. A small amount of the sample was deposited onto a "carbon-coated copper grid" with a mesh size of 400. The grid was then allowed to air-dry, after which it was subjected to "negative staining" using a 1% phosphotungstic acid solution. Following a 5 min incubation period, the copper grid was carefully inserted into the sample probe for TEM analysis, which was performed at an acceleration voltage of 200 kV.

Differential scanning colorimetry (DSC)

The DSC thermogram of drug substance, blank NPs, CH-NPs, and Tf-CH-NPs of ZH was determined utilizing the Perkin Elmer pyris 6 DSC, Massachusetts, USA. The NPs were placed in aluminium pans, securely sealed, and subjected to scanning using a differential scanning calorimeter. The scanning process involved heating the samples from 40 °C to 400 °C at a rate of 5 °C/min, all under an inert environment using nitrogen.

Fourier transform infrared spectroscopy (FTIR)

The drug material, blank NPs, CH-NPs, and Tf-CH-NPs of ZH were all subjected to FTIR spectra analysis using a Perkin Elmer FTIR spectrometer. To prepare the samples, a 1:100 ratio of dry Potassium Bromide (KBr) to sample was then powdered. These ready-made samples were subsequently put into sample cells and subjected to 20 scans at a resolution of 4 cm-1 within the 4700–400 cm-1 region.

X-ray diffraction (XRD)

Using a Bruker 8 diffractometer, the drug ingredient, CH-NPs, and Tf-CH-NPs of ZH were subjected to X-ray diffraction examination. The samples were exposed to Cu Kα X-ray radiation while being held in a sample holder for examination. Using a Goniometer detector, the scanning procedure encompassed a range of 5 to 50° 2 θ with a step size of 0.0080, and step time of 8.2550.

Entrapment efficiency (EE) and drug loading capacity (DLC)

The Tf-CH-NPs and CH-NPs containing ZH underwent centrifugation at 12000 rpm for a duration of 30 min. The resulting supernatant was then gathered, mixed with methanol to create a dilution, and subsequently examined at a wavelength of 318 nm [7], using a UV spectrophotometer to determine the concentration of the unbound drug. In a similar manner, the Drug Loading Capacity (DLC) was assessed based on the weight of the nanoparticle formulation. The Entrapment Efficiency (EE) and DLC were computed utilizing the subsequent formulas [19].

"Entrapment Efficiency (EE%) = [(Total Drug-Free drug)/Total drug] x 100"

"Drug Loading Capacity (DLC) = [(Total Drug-Free drug)/nanoparticle weight] x 100"

***In vitro* drug release study**

Prior to conducting the *in vitro* studies, the dialysis membrane underwent an activation process to eliminate any remaining sulphur salts and glycerine that may have been present due to the manufacturing process, as well as to open the pores of the membrane. The membrane was subjected to a continuous flow of running water for a duration of 3-4 h to eliminate any traces of glycerine residue. Subsequently, the membrane was exposed to a 0.3% w/v sodium sulphide solution at a temperature of 80 °C for a period of 1 minute, followed by a thorough rinsing with hot water for 2 min at a temperature of 60 °C. Furthermore, acidification was carried out using a 0.2% v/v sulphuric acid solution, and the membrane was then treated with hot water to remove any remaining acid and to ensure the absence of sulphate salts. This treatment protocol resulted in the retention of most proteins with a molecular weight equal to or greater than 12000 within the membrane [19, 20].

The drug release studies for ZH were conducted using activated dialysis bags. The bags contained CH-NPs, Tf-CH-NPs formulation, and a Drug Suspension (DS) of ZH (1 ml solution with 1 mg concentration). These samples were suspended in the dialysis bag and placed in 100 ml phosphate buffer solutions with pH values of 6.4, which served as the dissolution medium. The bag was maintained at 37 °C and then subjected to constant stirring at 100 rpm using a magnetic stirrer. At predetermined time intervals up to 24 h, sample aliquots were collected and analysed using Ultra Violet spectroscopy at 318 nm for drug concentration [7]. The percentage of drug release was calculated using the provided equation below [21],

$$\%\ \text{Drug release} = \frac{\text{Conc. (µg/ml)} \times \text{Dilution factor} \times \text{Volume of the release medium}}{\text{Initial dose (µg)}}$$

Ex vivo permeation study on nasal mucosa

Franz diffusion cells were used in the study, and goat nasal tissue samples showed a 0.785 cm^2 permeation area at the donor and receptor chamber contact. A pH 6.4 phosphate buffer containing 10 ml was added to the receptor chamber. The chamber was filled with a mixture of 95:05 ratio of oxygen and carbon dioxide, and the temperature was kept at 37± 2 °C. A pre-incubation period of 20 min was observed. The donor chamber (5 ml) contained a standard drug solution, ZH-CH-NPs, and ZH-Tf-CH-NPs, all equivalent to 0.5 mg of ZH. Samples of 1 ml were withdrawn from the receptor chamber at 0.25, 0.5, 1, 2, 4, 8, and 12 h, with an equivalent amount of phosphate buffer at pH 6.4 added back [22, 23]. The collected samples were filtered and subjected to analysis using the high-pressure liquid chromatography (HPLC) method [24].

Force of mucoadhesion of NPs

Force of Mucoadhesion of the formulations were evaluated by modified physical balance technique, a published method of *Kaushik Suhagiya et al.* with minor adjustments [22]. In this investigation, the

mucoadhesive properties of formulations with "goat nasal mucosa" were investigated. To simulate the nasal environment, the mucosa was soaked in 6.4 pH simulated nasal fluid. Subsequently, the mucosa was sandwiched between two glass slides, and the nanoparticle formulation was applied between them by gently pressing with a fingertip for 30 sec. To calibrate the physical balance, a glass beaker was placed on the opposite end. Then, water was gradually added from a burette, and the amount of water needed to separate the two slides was measured and recorded. The mucoadhesive strength was determined using a specific equation.

$$\text{Mucoadhesive Strength} = \frac{\text{Detachment weight (m)}}{\text{Area exposed (A)}} \times \text{Acceleration due to gravity (g)}$$

Histomorphology of nasal mucosa

Histomorphology was performed to evaluate the safety of optimized nanoformulations on the nasal mucosa integrity. Excised goat nasal mucosa obtained from local butcher was taken and cut into pieces with uniform thickness. The pieces were treated with normal saline, ZH-solution, CH-NPs, and Tf-CH-NPs of ZH. After treatment, all pieces of mucosa were collected, washed with phosphate buffer, and kept overnight in formalin solution (10% v/v). Subsequently, the specimens were encased within paraffin wax and thin sections, measuring 4 µm in thickness, were meticulously sliced using a microtome. These sections were stained with "hematoxylin and eosin" and meticulously examined under an inverted microscope to assess any potential harm inflicted upon the nasal mucosa [23, 25-27].

Assessment of depth of permeation using confocal laser scanning microscopy

"Confocal microscopy" was used to determine the depth of penetration of NPs formulation through the nasal mucosa. ZH-solution, CH-NPs, and Tf-CH-NPs of ZH were treated with rhodamine 123, and the formulations were applied to the excised nasal mucosal membrane. The pH and temperature of the dissolution media were maintained at the same levels as those used in the *in vitro* permeation study. After a 2-hour treatment with formulations, the mucosa was removed and positioned on a slide with the inner side facing up. The penetration depth of the formulation was evaluated by examining the fluorescence signals. The intensity and depth of permeation along the z-axis were observed and quantified using "Confocal Laser Scanning Microscopy" (CLSM) with "LEICA TCS SPE" and "LAS AF software" [23, 28–30].

RESULTS AND DISCUSSION

The presence of hydroxyl groups in chitosan facilitates chemical modifications by enabling the attachment of side groups to these reactive hydroxyl sites, while preserving its biophysical characteristics [31]. The concentrations of chitosan, Sodium tripolyphosphate were optimized using the design of experiments (Box Behnken design) as per our earlier research [2]. To synthesize conjugated chitosan nanoparticles, it is necessary to modify the chitosan by introducing azide groups, resulting in azido-chitosan. Additionally, the transferrin molecule needs to undergo modification by incorporating an alkyne group. After modification, the modified chitosan and Transferrin were characterized qualitatively to confirm the azido-chitosan by NMR and IR (fig. 1, 2).

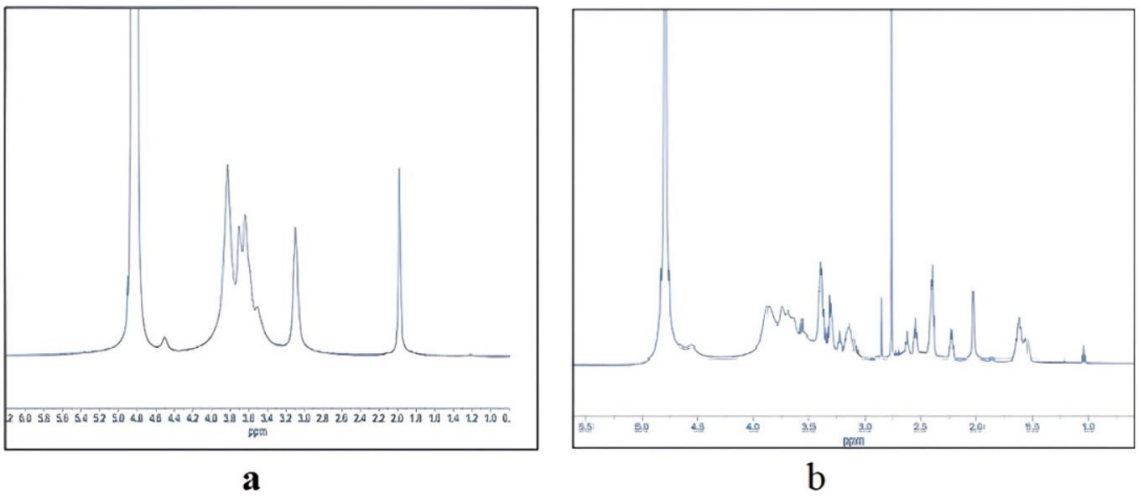

Fig. 1: NMR spectrum of chitosan a) Before modification, b) After modification

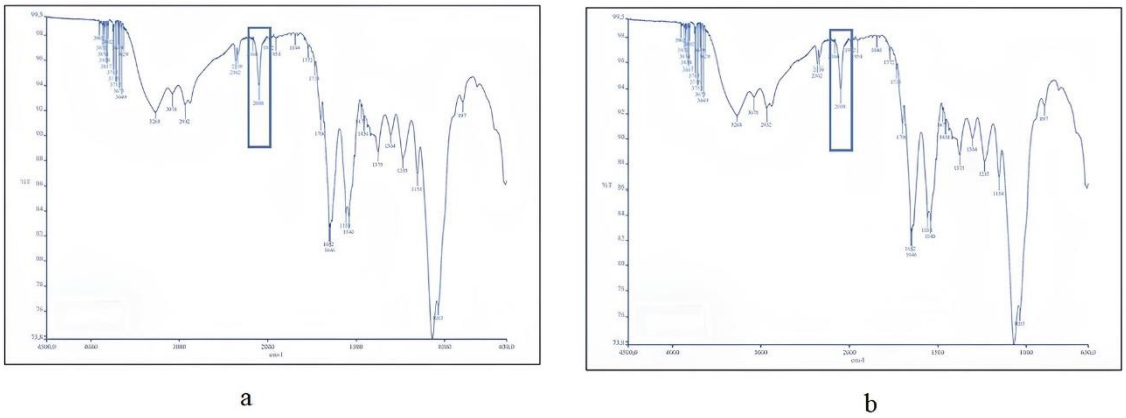

Fig. 2: Infra-red spectrum of chitosan a) Before modification, b) After modification and alkynation of Transferrin by gel electrophoresis (fig. 3)

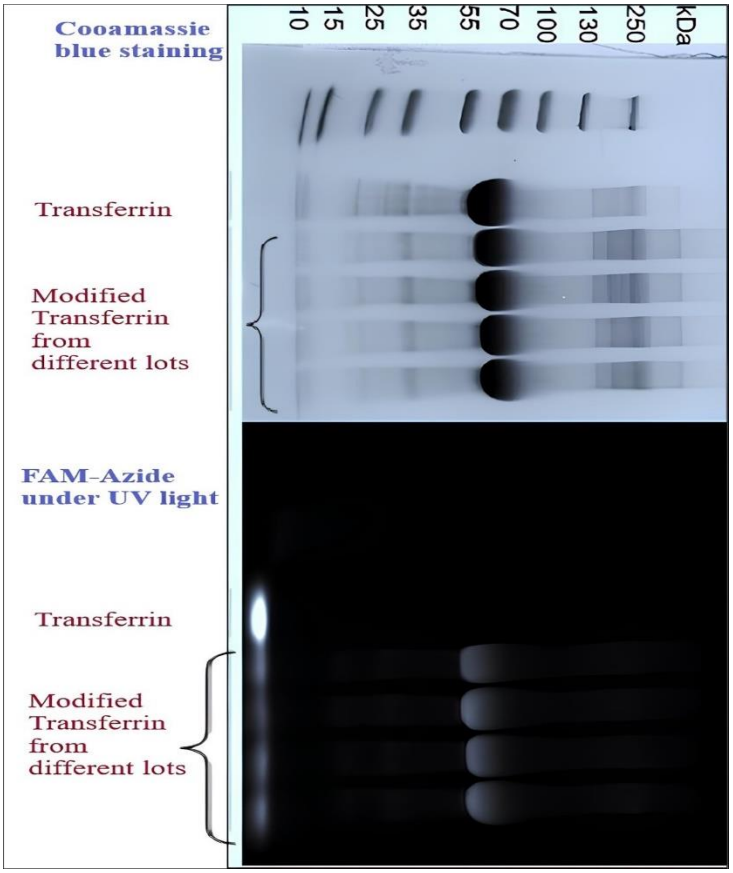

Fig. 3: Modified transferrin gel electrophoresis using coomassie blue staining and FAM-Azide under UV light

The NMR spectrum reveals the emergence of fresh signals and the division of protons, indicating a connection between 5-azidopentanoic acid and certain amino repeat units within chitosan. These findings point towards a triumphant alteration. The IR spectra of unaltered chitosan and chitosan modified with azide exhibit the emergence of absorbance at approximately 2100 cm^{-1} in the spectrum of the azide-modified CS. This particular absorbance is indicative of the presence of a terminal azide group.

To further investigate the impact of the modification, gel electrophoresis was performed (fig. 3). A comparison between alkyne-modified Tf and holo-Tf was conducted using "Coomassie staining". The results depicted in the fig. demonstrate that the protein bands of alkyne-Tf closely resemble those of unmodified Tf, indicating that the protein's integrity remains intact following the chemical alteration. Gel visibility under UV light following the click-reaction with FAM-azide provides proof of a successful alteration. The band of modified transferrin and the excess fluorescent reaction partner at the bottom of the gel become visible under UV light as a result of the click-reaction with FAM-azide. The fluorescent bands exhibit the same molecular weight as those observed in Coomassie staining, confirming that the illuminated substance is indeed modified-Tf with the fluorescent label. Notably, fluorescence is only detected at the" bottom of the gel" in the control sample, indicating that no conjugation occurred with unmodified holo-Tf.

The ligand conjugation of nanoparticles was confirmed by Surface Plasmon Resonance (SPR) (fig. 4) spectroscopy and DSC (fig. 5a), FTIR (fig. 5b), XRD (fig. 5c).

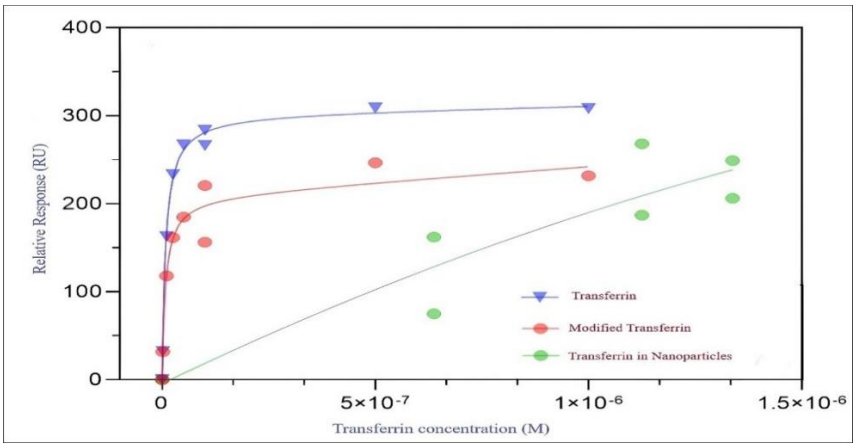

Fig. 4: SPR spectroscope of transferrin before and after modification and in nanoparticles

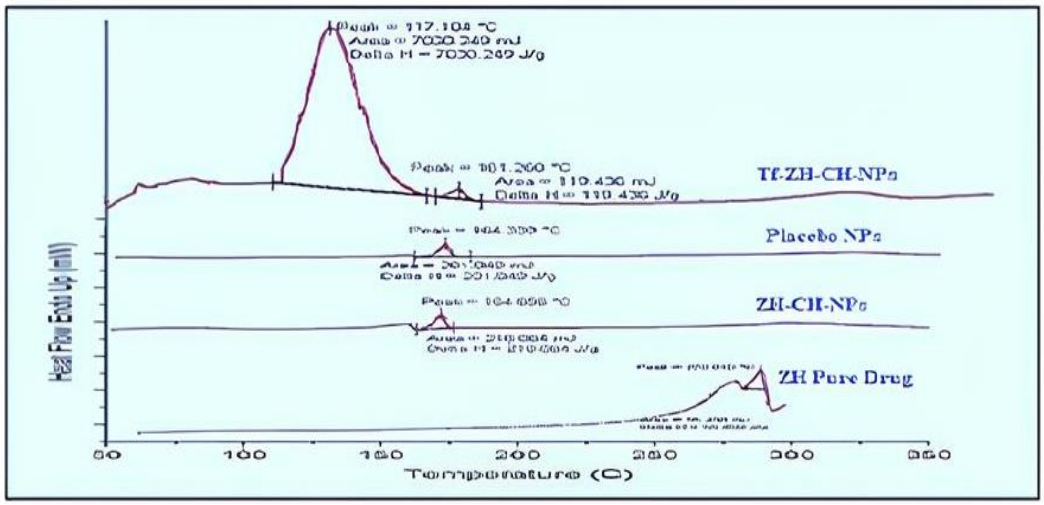

a

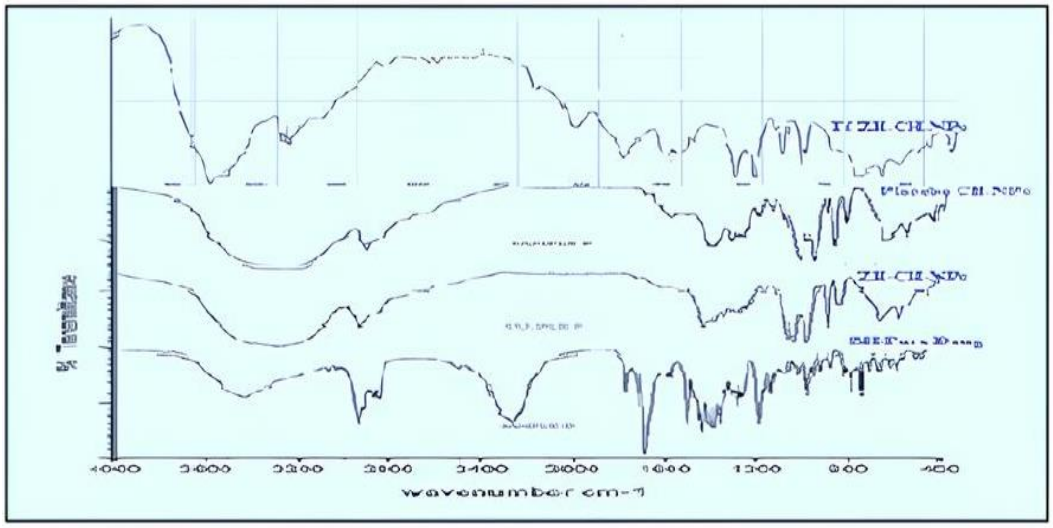

b

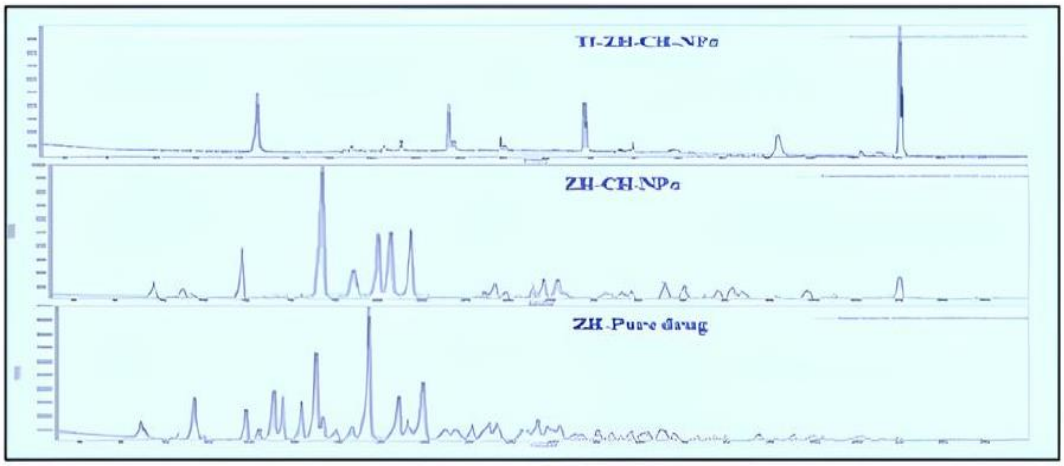

c

Fig. 5. a) DSC thermogram, b) FTIR spectrum and c) XRD of formulations

Tf underwent modification using "DBCO-NHS-ester". Under physiological conditions or slightly alkaline circumstances, this NHS ester-activated DBCO reacts with primary amines to produce stable amide bonds. Analysis using IR measurements did not reveal any discernible difference between Tf and alkyne-modified Tf. Moreover, this method was unable to detect the distinctive resonances of DBCO at 1710 cm−1 and 760 cm−1. The prepared Tf-decorated CH-NPs were analysed for their binding affinities using SPR spectroscopy.

The solutions of transferrin at a range of 1-5 mg were incorporated into nanoparticles to investigate the binding interactions. Chitosan was injected as a control at a similar concentration. The chemical modification of transferrin did not affect its binding behaviour to the transferrin receptor. The results showed differences in binding behaviour, with a higher interaction observed as the surface amount of transferrin per nanoparticle increased. A linear correlation curve showed that, despite the nanoparticle samples not reaching saturation, the binding was nonetheless discernible and not specific.

The resulting nanoparticles were evaluated for hydrodynamic diameter, homogeneity, zeta potential and encapsulation efficiency. An average diameter of 154.8 nm was increased to 207.1 nm after ligand conjugation. There is an increase in size and PDI with ligand-conjugated nanoparticles. Increased size can be attributed to the ligand molecular weight of about 80kDa, and higher PDI values due to lower control levels in the process of NP formation, which may also result in a variable amount of available Tf binding sites on the particle surface which is likely non-homogenous distribution of targeting ligand [13].

The formulation with a particle density of less than 0.5 had a homogeneous distribution [32]. The possible reason for lesser homogenous formulation is the inadequate control of NP formation via ionotropic gelation method. To analyze the surface properties and stability of NPs zeta potential was determined. It assesses the stability of NPs by measuring the charge on their surface. CH-NPs exhibited a comparatively higher zeta potential in comparison to Tf-ZH-CH-NPs. This difference in zeta potential can be attributed to the positive charge of chitosan being diminished by the shielding effect of the transferrin ligand. Nevertheless, the positive charge of chitosan was still adequate to uphold the stability of the formulation. Based on these outcomes, the 1 mg/ml concentration of modified ligand concentration was utilized for the trials considering their lower particle size in combination of better homogeneity and optimum encapsulation efficiency as per table 1.

Table 1: Optimization of transferrin concentration

Transferrin (mg/ml)	Hydrodynamic diameter in nm	PDI	Zeta potential in mV	Encapsulation efficiency in %
Plain Chitosan nanoparticles without Tf	154.8±4.0	0.443 ±0.054	33.7±4.72	88.5±0.05%
1 mg	207.1± 5.43	0.411± 0.065	28.7±3.0	87.6±0.06 %
2 mg	218.4±3.58	0.429±0.087	27.3±4.22	84.4±1.56 %
2.5 mg	217.8±4.34	0.445±0.043	26.4±2.58	82.6±1.98 %
4 mg	236.0±5.22	0.467±0.045	25.3±2.46	77.8±0.59 %
5 mg	243.5±3.67	0.483±0.079	24.5±2.33	76.7±2.03 %

All data showed as mean±SD (n=3); where n is the number of observations

Table 2: Physicochemical characterization of nanocarriers before and after conjugation with Transferrin

Parameter	Chitosan NP before Tf conjugation	Transferrin conjugated chitosan NP
Mean particle size (nm)	154.8±4.0	207.1± 5.43
Polydispersity Index	0.443 ±0.054	0.461±0.065
Zeta Potential (mV)	33.7±4.72	28.7±3.0
Encapsulation efficiency (%)	88.5±0.05%	87.6±0.06 %
Drug Loading Capacity (%)	8.8±0.07%	7.6± 0.06 %
Force of mucoadhesion (N)	0.17624±0.012	0.17089±0.043

All data showed as mean±SD(n=3); where n is the number of observations

The higher the % EE and DLC, the therapeutic efficacy of prepared formulation. From physicochemical characterization as per table 2 of formulations, it was concluded that with conjugation there is no significant drug-polymer interaction but shown a slight decrease in both entrapment and loading capacity after conjugation with ligand. NPs without ligand i. e., CH-ZH-NP, exhibited a slightly greater efficiency in encapsulation compared to NPs adorned with Tf. This discrepancy may arise from a reduction in the total number of charges within the CH molecule following chemical alterations. However, it should be emphasized that within the confines of this study, this trend does not hold statistical significance. Additionally, it is noteworthy that an escalation in the amount of Tf added does not yield a significant impact on the diameter of the NP, their zeta-potential, or their encapsulation efficiency.

DSC analysis of NPs formulation (fig. 5a) both placebo and drug loaded CH-NPs exhibited a distinct peak at 162 °C, corresponding to mannitol (165 °C) present in the formulation. ZH's DSC thermogram showed an endothermic peak at 285 °C, which is in close proximity to ZH's melting range and crystalline state. Tf-ZH-CH-NPs displayed two characteristic peaks at 117 °C, corresponding to Tf, and at 161.2 °C, corresponding to mannitol (165 °C). However, in the case of placebo and drug-loaded NPs, the drug peak was absent, suggesting complete entrapment of the drug within the polymeric nanoparticles. Additionally, variations in particle size influenced the endothermic peak, as different NPs melted at different temperatures, leading to peak broadening and shifting of the endotherm [33].

The FTIR spectrum of ZH-CH-NPs, (fig. 5b) displayed an absence of the characteristic peaks of drugs in comparison to the pure drug spectra. The reason for this is that ZH is completely entrapped in the NPs formulation. While Tf-ZH-CH-NPs spectra showed peak at 1566 and 1242 cm-1 that corresponds to the bending of N-H in the plane and the stretching of C-N in the amide II region are responsible for certain molecular vibrations in peptide linkages. Similarly, the stretching of C-N and the bending of N-H contribute to the molecular vibrations observed in the amide III region are corresponds to that of Transferrin. Moreover, additional absorption bands at 3454 (C-H stretching), 1211, and 883 cm-1 belongs to (NH2) out plane bending and stretching vibrations, which may be attributed to β-1,4 glucoside bond of CH. Absorption bands at 1080 cm-1 due to C-O-C stretching confirms the Tf conjugation to ZH-CH-NPs [13, 33].

In XRD analysis (fig. 5c), ZH showed distinct sharp diffraction peaks at 2Θ values of 11.36°, 13.89°, 15.12°, 17.06°, 19.66°, 20.74°, 21.90°, 27.38°, and 39.29° revealing crystalline nature of ZH. ZH-CH-NPs depicts sharp diffraction peak at 9.28°, 13.58°, 17.28°, 19.48°, 20.58°, 21.28° and 43.98° which may be attributed due to the presence of CH (9.28°, 20.58°, 21.28°) and mannitol in the formulation. Tf-conjugated NPs showed sharp diffraction peak at 14.75°, 23.41°, 28.64° and 44.12° (the presence of different peaks may be due to presence of Tf, CH and mannitol). Both CH-NPs and Tf-conjugated NPs of ZH showed absence of drug characteristics diffraction peaks indicating loss of crystallinity due to entrapment of drug within the NPs [34].

Surface topography was assessed using (TEM) (fig. 6).

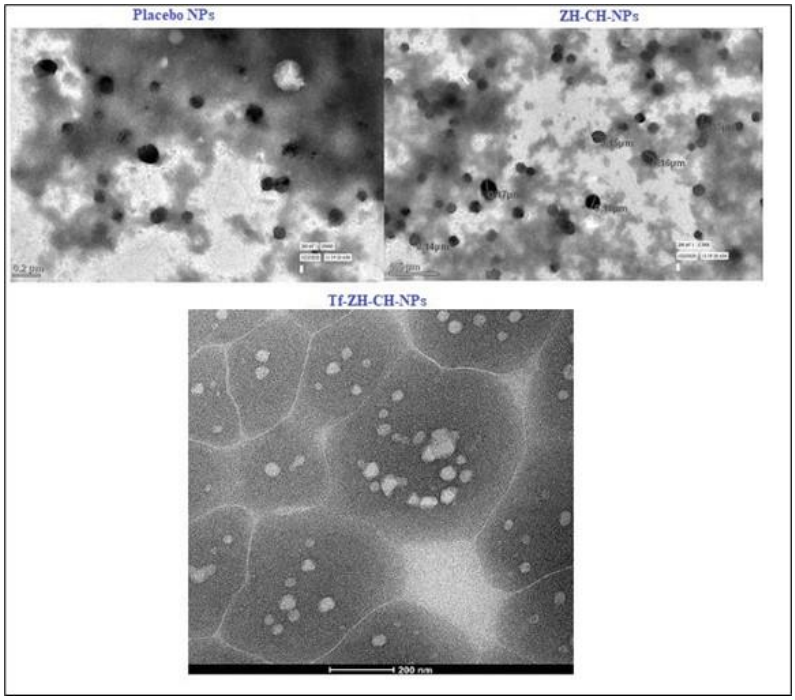

Fig. 6: TEM images of formulations

The TEM images revealed nanoparticles with a spherical shape and a diameter ranging from 140-170 nm, consistent with the size measured by the particle size analyzer. The TEM images also demonstrated that the particle size of Tf-ZH-CH-NPs fell within the range of 200-300 nm, which correlated with the results obtained from the particle size analyzer. In addition, there was no indication of NP aggregation in the pictures, which showed a uniform dispersion of particles [34]. Both the placebo and drug-loaded formulations exhibited particle sizes within a similar range, suggesting that the system was appropriate for the study.

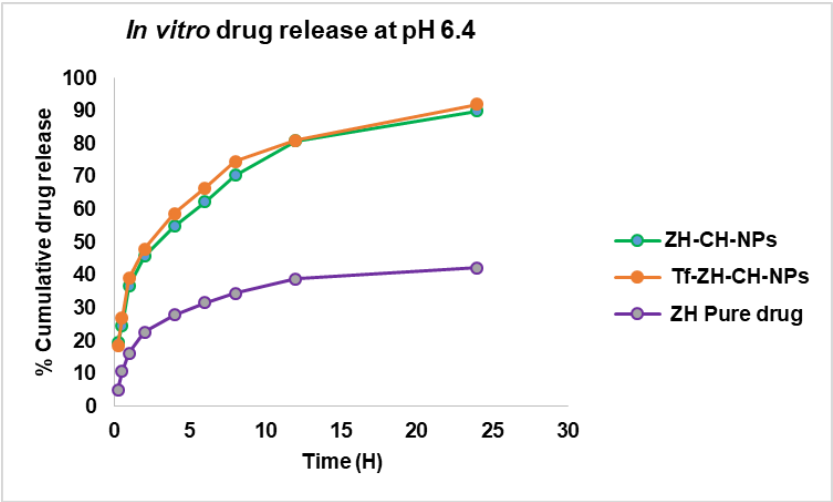

Fig. 7: *In vitro* drug release of NP formulations and pure drug suspension. Error bars were omitted

In vitro drug release study (fig. 7) reveals that, after 24 h, there was a release of 85.83±3.21% and 89.34±5.65% from ZH-CH-NPs and Tf-ZH-CH-NPs but only 40.22±2.76% from the drug suspension indicating 2.22 times that of drug suspension. Interestingly, there was a slightly higher drug release from ligand conjugated NPs. The drug release follows the First order drug release profile.

The total quantity of drug that penetrated through the nasal mucosa in the Ex vivo Nasal Permeation investigation (fig. 8) was 2.58±0.13 and 2.72±5.32 x10-2 µg/cm2/h after 6 h from drug-loaded CH-NPs and Tf-CH-NPs, respectively, whereas the permeation from ZH suspension was assessed to be 1.02±0.091x10-2 µg/cm2/h. The results demonstrated a 2.5-fold and 2.7-fold higher nasal permeation of ZH from CH-NPs and Tf-CH-NPs formulation, respectively, in comparison to the pure drug suspension. In contrast, NPs exhibited no crystallinity or aggregation, leading to increased permeability. The nasal mucosal membrane's lipophilic composition reduces the permeability of intact drug molecules by acting as a barrier to drug molecule penetration.

The force of mucoadhesion for optimized placebo and ZH-CH-NPs and Tf-ZH-CH-NPs were calculated. The placebo CH-NPs showed mucoadhesive strength of 0.1836±0.027 N, whereas ZH-CH-NPs and Tf-ZH-CH-NPs demonstrated 0.17624±0.012 N and 0.17089±0.043

N. The mucoadhesion of the placebo NPs was observed to have increased, primarily due to the enhanced availability of CH for interaction with mucin. Consequently, the reduced mucoadhesion of ZH-CH-NPs and Tf-ZH-CH-NPs can be attributed to the lower quantity of CH available for interaction with mucin. Additionally, the slight disparity in size between the placebo NP and the prepared NP formulations somewhat hinders the penetration of ZH into the mucosal layer. This can be attributed to the presence of a smaller amount of CH available for interaction with mucin. Furthermore, an increase in the particle size of nano sized particles would result in a decrease in the adsorption of mucin on the surface of the NPs, ultimately leading to a decreased mucoadhesive strength of the NPs.

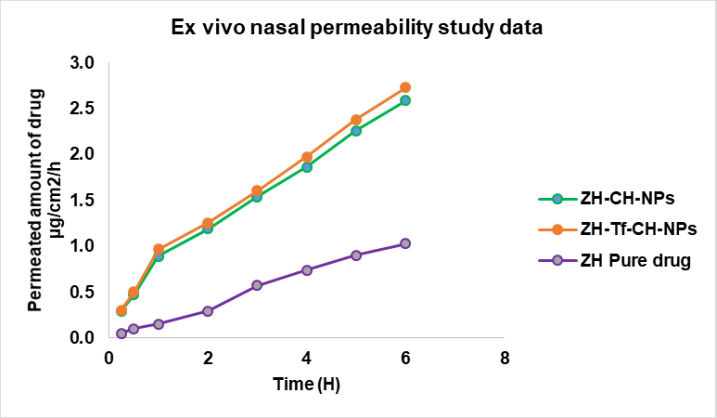

Fig. 8: *Ex vivo* nasal permeability of formulations. Error bars were omitted

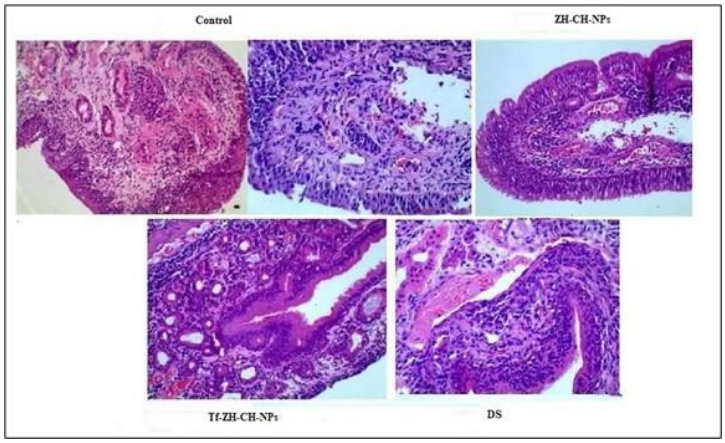

Fig. 9: Histomorphology of formulations

The findings from histomorphology examination (fig. 9) indicate the integrity and structure of the mucosa remained intact when treated with normal saline. Similarly, the mucosa treated with NPs did not exhibit any structural damage or signs of cell necrosis, indicating the safety of these nanoformulations. Furthermore, the nasal mucosa treated with nanoformulations showed minimal inflammation, suggesting that the developed formulation is biocompatible. These results can be attributed to the pH value of the nanoformulations, which falls within the range of the nasal mucosa pH value, 5.0-6.5, indicating the safety of the developed formulations for nasal administration. These findings align with the results obtained by *Shah et al*, who investigated the safety of Quetiapine NPs following nasal administration [25].

NPs successfully facilitated the transportation and distribution through the mucosal epithelium and sub-mucosal layers, as evidenced by the fluorescence intensity measurements (fig. 10).

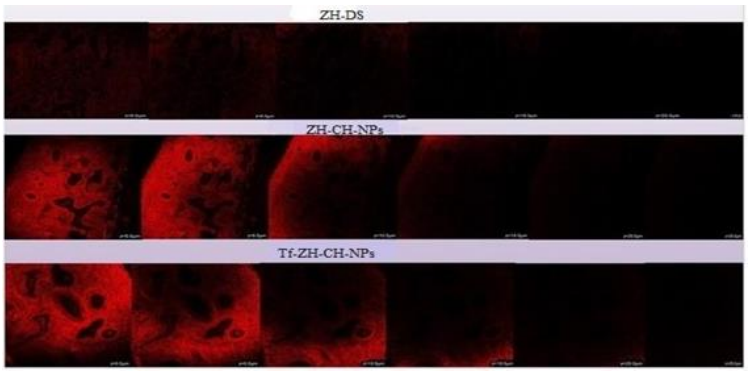

Fig. 10: Permeation depth of formulations in confocal microscopy

The movement of fluorescent labelled Drug Substance (DS) was confined to the upper mucosal layer, with a Z-average value of 5 µm. In contrast, ZH-CH-NPs and Tf-ZH-CH-NPs exhibited the transportation of the labelled compound to the sub-mucosal layers of the nasal epithelium, with Z-average values of 20 µm and 25 µm, respectively. ZH-CH-NPs and Tf-ZH-CH-NPs demonstrated superior transportation and permeation across the nasal epithelium when compared to the pure drug suspension. Furthermore, the NPs formulations exhibited deeper penetration across the nasal mucosa in comparison to pure DS. These findings suggest promising *in vivo* potential of NPs in enhancing the brain bioavailability of ZH when encapsulated in NPs, conjugated to Tf, and administered via the nasal route.

CONCLUSION

In this present study, we successfully developed Transferrin conjugated, ZH-loaded chitosan nano sized particles (Tf-ZH-CH-NPs) with desirable entrapment efficiency, particle size and sustained drug release up to 24 h. ZH-CH-NPs were prepared with modified chitosan and Transferrin by ionic gelation method and have demonstrated better *in vitro* release profile, *ex vivo* nasal permeation ability along with sufficient mucoadhesive strength and physiological acceptability to deliver via nasal route suitable for once daily administration. The confocal microscopy data revealed the distribution of labelled compound was deeper than unconjugated NPs, which shows the formulation has the potential to targeting delivery of drug to cerebrum. Thus, Tf-ZH-CH-NPs are promising in providing better treatment to schizophrenia patients with minimal doses that can be efficiently delivered to cerebrum and enables targeted delivery with reduced extrapyramidal side effects in a non-invasive manner and enhanced patient convenience.

ABBREVIATIONS

g: Gram; mg: Milli Gram; µg: Micro Gram; ml: Milli Liter; RC: Regenerated Cellulose; KD; Kilo Dalton; mm: Milli Meter; cm: Centi Meter; % w/w: Percentage Weight By Weight; µL: Micro Litre; °C: Degree Centigrade; mmol: Milli Moles; rpm: Revolutions Per Minute; µm: Micrometre; nm: Nanometre; mPa. s: Milli Pascal-Second; kV: Kilo Volt; min: Minute; cm^{-1}; Per Centimetre.

FUNDING

Nil

AUTHORS CONTRIBUTIONS

Ponduri Teja Kumar, Guntupalli Chakravarthi, Jeganathan Balamurugan have contributed for designing the concept. Ponduri Teja Kumar has performed the experimentation and written the manuscript. Guntupalli Chakravarthi, Jeganathan Balamurugan has supervised the work, findings of the work. Malothu Narender has reviewed the manuscript. All authors discussed the results and contributed to the final manuscript.

CONFLICT OF INTERESTS

Declared none

REFERENCES

1 Velligan DI, Rao S. The epidemiology and global burden of schizophrenia. J Clin Psychiatry. 2023 Jan 18;84(1):MS21078COM5. doi: 10.4088/JCP.MS21078COM5, PMID 36652681.
2 Kumar PT, Chakravarthy G, Balamurugan J. Design optimization and evaluation of intranasal nanotherapeutic of atypical antipsychotic drug. Eur Chem Bull. 2023 Dec 15;12:(si4). doi: 10.21203/rs.3.rs-3751418/v1.
3 Abo El Enin HA, Tulbah AS, Darwish HW, Salama R, Naguib IA, Yassin HA. Evaluation of brain targeting and antipsychotic activity of nasally administrated ziprasidone lipid polymer hybrid nanocarriers. Pharmaceuticals (Basel). 2023 Jun 15;16(6):886. doi: 10.3390/ph16060886, PMID 37375832.
4 Patil M, Patil J, Patil D, Patel K, Tatiya A. Significance of ziprasidone nanoparticles in psychotic disorders. MDPI. 2023 May 5;14(1):62. doi: 10.3390/IOCN2023-14503.
5 Alexander A, Agrawal M, Bhupal Chougule M, Saraf S, Saraf S. Nose to brain drug delivery. In: Nanopharmaceuticals. Elsevier; 2020. p. 175-200.
6 Illum L. Intranasal delivery to the central nervous system. In: Blood-brain barrier in drug discovery. Wiley; 2015. p. 535-65.
7 Mathrusri Annapurna M, Malavika V. New spectrophotometric methods for the estimation of ziprasidone an antipsychotic drug. Res J Pharm Technol. 2022 Jul 29:15(7):3209-12. doi: 10.52711/0974-360X.2022.00538.
8 Bahadur S, Pathak K. Buffered nanoemulsion for nose to brain delivery of ziprasidone hydrochloride: preformulation and pharmacodynamic evaluation. Curr Drug Deliv. 2012 Oct 1;9(6):596-607. doi: 10.2174/156720112803529792, PMID 22788695.
9 Gandhi S, Shastri DH, Shah J, Nair AB, Jacob S. Nasal delivery to the brain: harnessing nanoparticles for effective drug transport. Pharmaceutics. 2024 Apr 1;16(4):481. doi: 10.3390/pharmaceutics16040481, PMID 38675142.
10 Moreira R, Nobrega C, DE Almeida LP, Mendonca L. Brain targeted drug delivery nanovesicles directed to specific brain cells by brain targeting ligands. J Nanobiotechnology. 2024 May 17;22(1):260. doi: 10.1186/s12951-024-02511-7, PMID 38760847.
11 Anju G, Rupa M, Kamla P. Formulation optimization and characterization of ziprasidone nanocrystals prepared by media milling technique. Int J Pharm Pharm Sci. 2015 Jun 15;7(8):146-50.
12 Shehu IA, Shehu UM, Datta A. Intranasal delivery in managing antibiotic resistance in brain infections. Int J Curr Pharm Sci. 2022 Mar 15;14(2):1-4. doi: 10.22159/ijcpr.2022v14i2.1559.
13 Gabold B, Adams F, Brameyer S, Jung K, Ried CL, Merdan T. Transferrin modified chitosan nanoparticles for targeted nose to brain delivery of proteins. Drug Deliv Transl Res. 2023 Mar 7;13(3):822-38. doi: 10.1007/s13346-022-01245-z, PMID 36207657.
14 Anseth KS, Klok HA. Click chemistry in biomaterials nanomedicine and drug delivery. Biomacromolecules. 2016 Jan 11;17(1):1-3. doi: 10.1021/acs.biomac.5b01660, PMID 26750314.
15 Meldal M, Tornoe CW. Cu-catalyzed azidealkyne cycloaddition. Chem Rev. 2008 Aug 1;108(8):2952-3015. doi: 10.1021/cr0783479, PMID 18698735.
16 Lunkov A, Shagdarova B, Lyalina T, Dubinnyi MA, Karpova N, Lopatin S. Simple method for ultrasound assisted click modification of azido chitosan derivatives by CuAAC. Carbohydr Polym. 2022 Apr;282:119109. doi: 10.1016/j.carbpol.2022.119109, PMID 35123745.
17 Dixit N, Trivedi A, Ahirwar D. Polyethylene glycol chitosan nanoparticle gel for the controlled nasal delivery of noscapine against glioma. Int J App Pharm. 2022 May 7;14(3):153-61. doi: 10.22159/ijap.2022v14i3.43779.
18 Pedroso Santana S, Fleitas Salazar N. Ionotropic gelation method in the synthesis of nanoparticles/microparticles for biomedical purposes. Polym Int. 2020 May 3;69(5):443-7. doi: 10.1002/pi.5970.
19 Nabi B, Rehman S, Fazil M, Khan S, Baboota S, Ali J. Riluzole loaded nanoparticles to alleviate the symptoms of neurological disorders by attenuating oxidative stress. Drug Dev Ind Pharm. 2020 Mar 3;46(3):471-83. doi: 10.1080/03639045.2020.1730396, PMID 32057274.
20 Annu BS, Baboota S, Ali J. *In vitro* appraisals and ex vivo permeation prospect of chitosan nanoparticles designed for schizophrenia to intensify nasal delivery. Polym Bull. 2022 Apr 9;79(4):2263-85. doi: 10.1007/s00289-021-03598-w.
21 Jazuli I, Annu NB, Nabi B, Moolakkadath T, Alam T, Baboota S. Optimization of nanostructured lipid carriers of lurasidone hydrochloride using box behnken design for brain targeting: *in vitro* and *in vivo* studies. J Pharm Sci. 2019 Sep;108(9):3082-90. doi: 10.1016/j.xphs.2019.05.001, PMID 31077685.
22 Suhagiya K, Borkhataria CH, Gohil S, Manek RA, Patel KA, Patel NK. Development of mucoadhesive in situ nasal gel formulation for enhanced bioavailability and efficacy of rizatriptan in migraine treatment. Results in Chemistry. 2023 Dec;6:101010. doi: 10.1016/j.rechem.2023.101010.
23 Ahmed TA, Badr Eldin SM, Ahmed OA, Aldawsari H. Intranasal optimized solid lipid nanoparticles loaded in situ gel for enhancing trans mucosal delivery of simvastatin. J Drug Deliv Sci

Technol. 2018 Dec;48:499-508. doi: 10.1016/j.jddst.2018.10.027.

24 Bansal R, Chandrabose K, Hari Narayana Moorthy NS, Singh DP, Singh D, Trivedi P. A new simple and rapid validated RP-HPLC method for determination of ziprasidone in ziprasidone capsules. J Saudi Chem Soc. 2016 Sep;20:S161-7. doi: 10.1016/j.jscs.2012.10.005.

25 Shah B, Khunt D, Misra M, Padh H. Application of box-behnken design for optimization and development of quetiapine fumarate loaded chitosan nanoparticles for brain delivery via intranasal route. Int J Biol Macromol. 2016 Aug;89:206-18. doi: 10.1016/j.ijbiomac.2016.04.076, PMID 27130654.

26 Shah BM, Misra M, Shishoo CJ, Padh H. Nose to brain microemulsion based drug delivery system of rivastigmine: formulation and *ex-vivo* characterization. Drug Deliv. 2015 Oct 3;22(7):918-30. doi: 10.3109/10717544.2013.878857, PMID 24467601.

27 Khan K, Aqil M, Imam SS, Ahad A, Moolakkadath T, Sultana Y. Ursolic acid loaded intra nasal nano lipid vesicles for brain tumour: formulation optimization *in vivo* brain/plasma distribution study and histopathological assessment. Biomed Pharmacother. 2018 Oct;106:1578-85. doi: 10.1016/j.biopha.2018.07.127, PMID 30119233.

28 Hasan N, Imran M, Kesharwani P, Khanna K, Karwasra R, Sharma N. Intranasal delivery of naloxone loaded solid lipid nanoparticles as a promising simple and non invasive approach for the management of opioid overdose. Int J Pharm. 2021 Apr;599:120428. doi: 10.1016/j.ijpharm.2021.120428, PMID 33662465.

29 Wang M, Wang S, Zhang Y, Liu H, LI P, DU S. Studies of mucosal irritation and cellular uptake mechanisms of xingnaojing nanoemulsion. Braz J Pharm Sci. 2022;58:e20241. doi: 10.1590/s2175-97902022e20241.

30 Sun Y, LI L, Xie H, Wang Y, Gao S, Zhang L. Primary studies on construction and evaluation of ion-sensitive in situ gel loaded with paeonol solid lipid nanoparticles for intranasal drug delivery. Int J Nanomedicine. 2020 May 4;15:3137-60. doi: 10.2147/IJN.S247935.

31 .El Assal MI SD. Optimization of rivastigmine chitosan nanoparticles for neurodegenerative alzheimer; *in vitro* and ex vivo characterizations. Int J Pharm Pharm Sci. 2022 Jan 1;14(1):17-27. doi: 10.22159/ijpps.2022v14i1.43145.

32 Hoseini B, Jaafari MR, Golabpour A, Momtazi Borojeni AA, Karimi M, Eslami S. Application of ensemble machine learning approach to assess the factors affecting size and polydispersity index of liposomal nanoparticles. Sci Rep. 2023 Oct 21;13(1):18012. doi: 10.1038/s41598-023-43689-4, PMID 37865639.

33 Tiwari P. Mucoadhesive microspheres based formulation development of ziprasidone hydrochloride for nasal delivery. Int J Emerg Trends Sci Technol. 2017 Aug 30;4(8):5372-82. doi: 10.18535/ijetst/v4i8.03.

34 Jose S, A CT, Sebastian R, H SM, A AN, Durazzo A. Transferrin conjugated docetaxel PLGA nanoparticles for tumor targeting: influence on MCF-7 cell cycle. Polymers (Basel). 2019 Nov 19;11(11):1905. doi: 10.3390/polym11111905, PMID 31752417.